Rashba-like dispersion in buckled square lattices

A. S. Rodin,[1] P. Z. Hanakata,[2] A. Carvalho,[1] H. S. Park,[3] D. K. Campbell,[2] and A. H. Castro Neto[1]
[1]*Centre for Advanced 2D Materials and Graphene Research Centre, National University of Singapore, 6 Science Drive 2, 117546, Singapore*
[2]*Department of Physics, Boston University, Boston, Massachusetts 02215, USA*
[3]*Department of Mechanical Engineering, Boston University, Boston, Massachusetts 02215, USA*
(Received 22 March 2017; published 28 September 2017)

The band structure of a general class of buckled square lattice materials is investigated using *ab initio* calculations along with tight-binding modeling. We show that buckling and spin-orbit interaction give rise to a large Rashba-like splitting in the absence of an external electric field. The generality and the robustness of the effect make this class of materials promising candidates for spintronic applications.

DOI: 10.1103/PhysRevB.96.115450

I. INTRODUCTION

The spin-orbit interaction (SOI) occupies a special place in physics, where even its simplest manifestation is highly nontrivial, being relativistic in nature. In solid-state systems, SOI can be either extrinsic or intrinsic. Extrinsic systemwide SOI is generally described using the Rashba formalism, where a perpendicular electric field is applied to the system, leading to a lifting of band degeneracy.

Intrinsic SOI in two dimensions is only detected in materials with heavy elements, like some transition-metal dichalcogenides, or graphene-like buckled "X"enes. For both classes of materials, SOI results in band splitting, opening a gap [1–6]. In addition, a recent paper [7] used symmetry arguments to predict the properties of nodal materials arising from strong spin-orbit coupling.

In this work, we focus our attention on buckled square lattices with strong spin-orbit coupling. We show that unlike hexagonal lattices where SOC leads to level splitting and/or gap opening the K point, here, spin-orbit effects result in a Rashba-like dispersion even without an external electric field. It is worth noting that while this work is theoretical, the class of systems considered has very simple structures and can be constructed using existing technology [8,9]. In addition, we have performed *ab initio* calculations to show that the system in question is amenable to being grown on top of metallic substrates.

The paper is organized as follows. In Sec. II, we construct a tight binding model for a general buckled square lattice. Following this, we focus on two high-symmetry points of the Brillouin zone in Sec. III to show the appearance of the Rashba-like dispersion. Our results demonstrate that this dispersion is found at the M point even when the lattice is composed of a single atomic species with no dipole moment perpendicular to the system. At the Γ point, on the other hand, the Rashba-like bands arise only if the lattice contains two different types of atoms. We provide a numerical confirmation of our results in Sec. IV. Discussion and conclusions can be found in Sec. V.

II. TIGHT BINDING

In this section, we construct a tight-binding Hamiltonian for a general buckled square lattice involving s and p orbitals. The purpose of the tight-binding model is to provide an intuitive platform for understanding the microscopic origins of the Rashba-like dispersion. In the following section, we will consider Γ and M points of the Brillouin zone using a low-momentum expansion of the full Hamiltonian we obtain here.

To keep the number of hopping parameters to a minimum, we include only nearest neighbor hopping. We proceed by first neglecting spin-orbit effects in order to simplify the problem by focusing on a single spin.

A buckled square lattice is composed of two inequivalent shifted square sublattices A and B, as seen in Fig. 1. We set the bond length to a and the (buckling) angle that it makes with the horizontal to θ. This yields the unit cell size of $2\alpha a \times 2\alpha a$, where $\alpha = \cos\theta/\sqrt{2}$. From this, the dimensions of the Brillouin zone are $-\frac{\pi}{2\alpha a} \leqslant q_x, q_y \leqslant \frac{\pi}{2\alpha a}$. As a concrete example of such a lattice, Fig. 1 shows a buckled square lattice of lead atoms on top of bulk copper [100] surface.

Since we allow hopping only between nearest neighbors, in the absence of spin-orbit interaction, there is no coupling between different orbitals of the same sublattice. This means that in the basis of $(s,\ p_x,\ p_y,\ p_z)$, the onsite energies are given by

$$\Sigma_i = \begin{pmatrix} S_i & 0 & 0 & 0 \\ 0 & P_i & 0 & 0 \\ 0 & 0 & P_i & 0 \\ 0 & 0 & 0 & P_i \end{pmatrix}, \tag{1}$$

where S_i and P_i are s- and p-orbital energies for sublattice i.

To write down the hopping matrix, we use the following Slater-Koster matrix elements for the orbitals of neighboring atoms [10]:

$$\begin{aligned} &s\text{-}s : V_{ss\sigma}\,, \\ &s\text{-}p : V_{sp\sigma}\hat{d}\cdot\hat{o}_j\,, \\ &p\text{-}p : (\hat{o}_i\cdot\hat{o}_j)V_{pp\pi} + (\hat{o}_i\cdot\hat{d})(\hat{o}_j\cdot\hat{d})(V_{pp\sigma} - V_{pp\pi})\,. \end{aligned} \tag{2}$$

Here, $\hat{o}_i$ is the orientation of the ith orbital and $\hat{d}$ is the unit vector pointing from atom 1 to atom 2. This leads to the

following $A \to B$ hopping matrix:

$$K = 4\cos(k_x)\cos(k_y)\begin{pmatrix} V_{ss\sigma} & 0 & 0 & -\beta V^{(1)}_{sp\sigma} \\ 0 & V_{pp\pi}+\alpha^2\Delta & 0 & 0 \\ 0 & 0 & V_{pp\pi}+\alpha^2\Delta & 0 \\ \beta V^{(2)}_{sp\sigma} & 0 & 0 & V_{pp\pi}+\beta^2\Delta \end{pmatrix} - 4\alpha^2\Delta\sin(k_x)\sin(k_y)\begin{pmatrix} 0&0&0&0\\0&0&1&0\\0&1&0&0\\0&0&0&0\end{pmatrix}$$
$$+4\alpha\cos(k_x)\sin(k_y)\begin{pmatrix} 0 & 0 & iV^{(1)}_{sp\sigma} & 0 \\ 0 & 0 & 0 & 0 \\ -iV^{(2)}_{sp\sigma} & 0 & 0 & -i\beta\Delta \\ 0 & 0 & -i\beta\Delta & 0 \end{pmatrix} + 4\alpha\cos(k_y)\sin(k_x)\begin{pmatrix} 0 & iV^{(1)}_{sp\sigma} & 0 & 0 \\ -iV^{(2)}_{sp\sigma} & 0 & 0 & -i\beta\Delta \\ 0 & 0 & 0 & 0 \\ 0 & -i\beta\Delta & 0 & 0 \end{pmatrix}. \quad (3)$$

The dimensionless momentum $k_{x/y} = \alpha a q_{x/y}$ and $\beta = \sin\theta$. To keep the expression more compact, we have introduced $\Delta = V_{pp\sigma} - V_{pp\pi}$. In addition, since A and B species are not necessarily the same, we have two quantities of the $V_{sp\sigma}$ form.

While it is convenient to use s and p orbitals to write down the hopping matrix, since we are interested in including SOI in our model, it is helpful to go to a basis which is more natural for the angular momentum operators:

$$|0,0\rangle = |s\rangle\,, \quad |1,\pm1\rangle = \frac{\mp|p_x\rangle - i|p_y\rangle}{\sqrt{2}}\,, \quad |1,0\rangle = |p_z\rangle\,, \quad (4)$$

where the first number represents the orbital momentum quantum number and the second one is its projection along the $\hat{z}$ direction. This basis change does not alter the Σ matrices. The interlattice hopping portion of the Hamiltonian, on the other hand, becomes

$$\tilde{K} = 4\cos(k_x)\cos(k_y)\begin{pmatrix} V_{ss\sigma} & 0 & 0 & -\beta V^{(1)}_{sp\sigma} \\ 0 & V_{pp\pi}+\alpha^2\Delta & 0 & 0 \\ 0 & 0 & V_{pp\pi}+\alpha^2\Delta & 0 \\ \beta V^{(2)}_{sp\sigma} & 0 & 0 & V_{pp\pi}+\beta^2\Delta \end{pmatrix} + 4\alpha^2\Delta\sin(k_x)\sin(k_y)\begin{pmatrix} 0&0&0&0\\0&0&-i&0\\0&i&0&0\\0&0&0&0\end{pmatrix}$$
$$+2\sqrt{2}\alpha\sin(k_x)\cos(k_y)\begin{pmatrix} 0 & -iV^{(1)}_{sp\sigma} & iV^{(1)}_{sp\sigma} & 0 \\ iV^{(2)}_{sp\sigma} & 0 & 0 & i\beta\Delta \\ -iV^{(2)}_{sp\sigma} & 0 & 0 & -i\beta\Delta \\ 0 & i\beta\Delta & -i\beta\Delta & 0 \end{pmatrix} + 2\sqrt{2}\alpha\sin(k_y)\cos(k_x)\begin{pmatrix} 0 & V^{(1)}_{sp\sigma} & V^{(1)}_{sp\sigma} & 0 \\ V^{(2)}_{sp\sigma} & 0 & 0 & \beta\Delta \\ V^{(2)}_{sp\sigma} & 0 & 0 & \beta\Delta \\ 0 & -\beta\Delta & -\beta\Delta & 0 \end{pmatrix}. \quad (5)$$

In the following section, we will obtain simplified Hamiltonians for high-symmetry points of the Brillouin zone and include the atomic spin-orbit interaction in them.

III. EFFECTIVE HAMILTONIAN

Having constructed a tight-binding Hamiltonian for a general buckled system, we show how spin orbit coupling gives rise to the Rashba-like dispersion at the high-symmetry points of the Brillouin zone.

For the square Brillouin zone of our system, there are two particular points of interest: Γ and M. We will address them individually using a simplified version of $\tilde{K}$ from Eq. (5). Before we proceed, however, let us introduce the atomic spin-orbit coupling Hamiltonian:

$$H^i_{\rm SOC} = T_i\left(\frac{L_+\otimes s_- + L_-\otimes s_+}{2} + L_z\otimes s_z\right), \quad (6)$$

where $L_\pm$ and $s_\pm$ are the ladder operators for orbital and spin angular momenta, and L_z and s_z are the angular momentum operators in $\hat{z}$. The index i labels the sublattice.

The orbital angular momentum ladder operators are well suited for our new basis as they operate on the second quantum number in Eq. (4) to change it by one. Thus, the term of $H^i_{\rm SOC}$ with the ladder operators couples $|1,1\rangle\otimes|\downarrow\rangle$ with $|1,0\rangle\otimes|\uparrow\rangle$ and $|1,-1\rangle\otimes|\uparrow\rangle$ with $|1,0\rangle\otimes|\downarrow\rangle$ of the same sublattice with the coupling strength $T_{\rm SO}/\sqrt{2}$. The second term, one the other hand, modifies the diagonal elements of the self-energy for $|1,\pm1\rangle$ by adding (subtracting) $T_{\rm SO}/2$ if L_z and s_z point in the same (opposite) direction.

A. *M* point

We start by turning our attention to the M point, located at the corner of the Brillouin zone at $k_x = k_y = \pi/2$. As was stated earlier, we can show that the Rashba-like bands at the M point require only buckling and sufficiently strong SOI. In other words, this dispersion explicitly does not require a transverse electric field.

To the leading order in k, the hopping matrix $\tilde{K}$ becomes

$$\tilde{K} = 4\alpha^2\Delta\begin{pmatrix}0&0&0&0\\0&0&-i&0\\0&i&0&0\\0&0&0&0\end{pmatrix}$$
$$-2\sqrt{2}\alpha k\begin{pmatrix} 0 & V^{(1)}_{sp\sigma}e^{-i\phi} & V^{(1)}_{sp\sigma}e^{i\phi} & 0 \\ V^{(2)}_{sp\sigma}e^{i\phi} & 0 & 0 & \beta\Delta e^{i\phi} \\ V^{(2)}_{sp\sigma}e^{-i\phi} & 0 & 0 & \beta\Delta e^{-i\phi} \\ 0 & -\beta\Delta e^{-i\phi} & -\beta\Delta e^{i\phi} & 0 \end{pmatrix}, \quad (7)$$

where ϕ is the angle measured from the $\hat{x}$ direction. At $k = 0$, the Hamiltonian decomposes into several uncoupled blocks

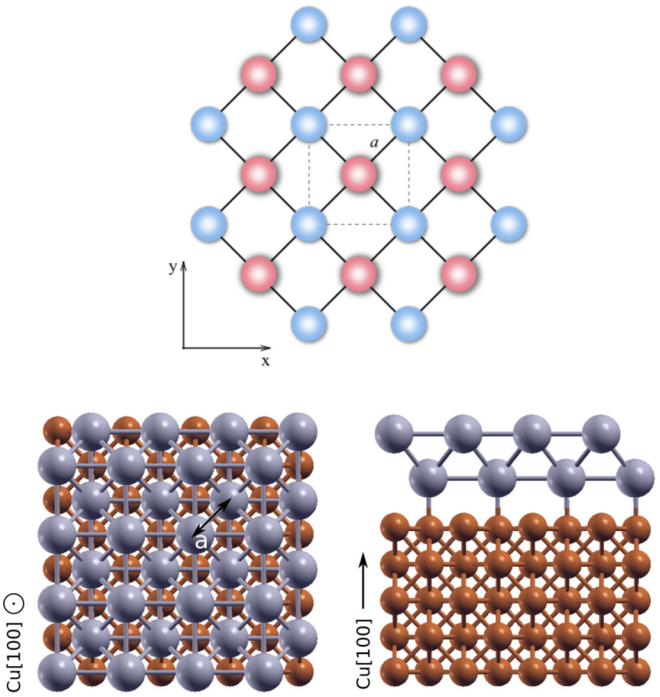

FIG. 1. (Top) Buckled square lattice with the two sublattices represented by the two different colors. The dashed square marks the unit cell. (Bottom) Pb buckled square lattice on top of bulk copper.

with the corresponding bases:

$$H_s^{m,\pm} = S_m : |0,0\rangle \otimes |\pm\rangle \otimes |m\rangle\,,$$
$$H_p^{mn,\pm} = \begin{pmatrix} P_m - \frac{T_m}{2} & \frac{T_m}{\sqrt{2}} & \mp 4i\alpha^2\Delta \\ \frac{T_m}{\sqrt{2}} & P_m & 0 \\ \pm 4i\alpha^2\Delta & 0 & P_n + \frac{T_n}{2} \end{pmatrix} : \begin{pmatrix} |1,\pm 1\rangle \otimes |\mp\rangle \otimes |m\rangle \\ |1,0\rangle \otimes |\pm\rangle \otimes |m\rangle \\ |1,\mp 1\rangle \otimes |\mp\rangle \otimes |n\rangle \end{pmatrix}, \quad (8)$$

where $m \neq n$ label the sublattices and the middle $|\pm\rangle$ ket denotes the spin state. Using the direct sum notation, we can write down the total Hamiltonian as $H = H_s^{A,+} \oplus H_s^{A,-} \oplus H_s^{B,+} \oplus H_s^{B,-} \oplus H_p^{AB,+} \oplus H_p^{AB,-} \oplus H_p^{BA,+} \oplus H_p^{BA,-}$.

From H_s, we see that for a given m, the eigenstates are spin degenerate. The degeneracy becomes fourfold if the atoms of sublattices A and B are the same, leading to $S_A = S_B$. Equation (7) shows that at finite k there is no coupling between the degenerate $|0,0\rangle$ states that is linear in momentum. This means that the bands composed of s orbitals have local extrema at the M point.

Next, we turn to H_p from Eq. (8). Just as for H_s, the bands are doubly or fourfold degenerate depending on whether the sublattices are composed of the same atomic species. Without making assumptions about the lattice composition, the general form of the degenerate states is

$$|\Psi^{\pm}\rangle_{mn} = a|1,\pm 1\rangle \otimes |\mp\rangle \otimes |m\rangle + b|1,0\rangle \otimes |\pm\rangle \otimes |m\rangle \pm ic|1,\mp 1\rangle \otimes |\mp\rangle \otimes |n\rangle\,, \quad (9)$$

with a, b, and c real. At finite k,

$${}_{mn}\langle\Psi^+|H|\Psi^-\rangle_{mn} = -2\sin 2\theta bc\left(\Delta ike^{-i\phi}\right)\varepsilon_{mn}\,, \quad (10)$$

where $\varepsilon_{AB} = -\varepsilon_{BA} = 1$ is the two-dimensional Levi-Civita symbol. This coupling between the degenerate states leads to an effective Rashba-like Hamiltonian:

$$H_{\text{eff}}^{mn} = 2\sin 2\theta bc\Delta\varepsilon_{mn}[(\mathbf{k}\times\sigma)\cdot\hat{z}] : \begin{pmatrix} |\Psi^+\rangle_{mn} \\ |\Psi^-\rangle_{mn} \end{pmatrix}. \quad (11)$$

It is important to keep in mind that the product bc in the Eq. (11) depends on the identities of the m and n sublattices and swapping them leads to a different bc. The Hamiltonian in Eq. (11) results in a linear dispersion which, when superimposed on the underlying curvature of the band at the M point, leads to a Rashba-like dispersion. The presence of $\sin 2\theta$ explicitly shows that for a flat lattice with $\theta = 0$, the prefactor of the Hamiltonian in Eq. (11) goes to zero, leading to a vanishing Hamiltonian. The upper and lower linear branches of Eq. (11) are given by

$$|U/L\rangle_{mn} = \frac{1}{\sqrt{2}}\begin{pmatrix} 1 \\ \pm\varepsilon_{mn} ie^{i\phi} \end{pmatrix}. \quad (12)$$

Just as with traditional Rashba states, the wave functions in Eq. (12) have spins pointing perpendicular to the momentum with the upper and lower branches manifesting opposite spins. In addition, it is straightforward to see that because of the Levi-Civita term in Eq. (11), the spin texture of the upper and lower branches of H_{eff}^{mn} is opposite to that of H_{eff}^{nm}. Generally, the energies of the $|U/L\rangle_{mn}$ and $|U/L\rangle_{nm}$ are not equal, resulting in a nonvanishing spin texture. If, however, the lattice is composed of a single atomic species, the bands of H_{eff}^{mn} and H_{eff}^{nm} become degenerate and their opposite spin orientation leads to the overall cancellation of the spin texture while retaining the linear dispersion.

B. Γ point

Next, we move to the Γ point at the center of the Brillouin zone. Unlike the M point, the Rashba-like dispersion appears only for heterogeneous lattices. Moreover, because of the band composition and the required coupling between different orbitals, the splitting here will generally be weaker than at the M point.

As before, we start by obtaining the simplified effective Hamiltonian. Here, $\tilde{K}$ does not undergo such a drastic simplification as at the corner of the Brillouin zone:

$$\tilde{K} = 4\begin{pmatrix} V_{ss\sigma} & 0 & 0 & -\beta V_{sp\sigma}^{(1)} \\ 0 & V_{pp\pi} + \alpha^2\Delta & 0 & 0 \\ 0 & 0 & V_{pp\pi} + \alpha^2\Delta & 0 \\ \beta V_{sp\sigma}^{(2)} & 0 & 0 & V_{pp\pi} + \beta^2\Delta \end{pmatrix} - 2\sqrt{2}i\alpha k\begin{pmatrix} 0 & V_{sp\sigma}^{(1)}e^{i\phi} & -V_{sp\sigma}^{(1)}e^{-i\phi} & 0 \\ -V_{sp\sigma}^{(2)}e^{-i\phi} & 0 & 0 & -\beta\Delta e^{-i\phi} \\ V_{sp\sigma}^{(2)}e^{i\phi} & 0 & 0 & \beta\Delta e^{i\phi} \\ 0 & -\beta\Delta e^{i\phi} & \beta\Delta e^{-i\phi} & 0 \end{pmatrix}. \quad (13)$$

For $k = 0$, we get the following uncoupled Hamiltonian blocks:

$$H_1^{\pm} = \begin{pmatrix} S_A & 0 & 0 & 4V_{ss\sigma} & 0 & -4\beta V_{sp\sigma}^{(1)} \\ 0 & P_A - \frac{T_A}{2} & \frac{T_A}{\sqrt{2}} & 0 & 4V_{pp\pi} + 4\alpha^2\Delta & 0 \\ 0 & \frac{T_A}{\sqrt{2}} & P_A & 4\beta V_{sp\sigma}^{(2)} & 0 & 4V_{pp\pi} + 4\beta^2\Delta \\ 4V_{ss\sigma} & 0 & 4\beta V_{sp\sigma}^{(2)} & S_B & 0 & 0 \\ 0 & 4V_{pp\pi} + 4\alpha^2\Delta & 0 & 0 & P_B - \frac{T_B}{2} & \frac{T_B}{\sqrt{2}} \\ -4\beta V_{sp\sigma}^{(1)} & 0 & 4V_{pp\pi} + 4\beta^2\Delta & 0 & \frac{T_B}{\sqrt{2}} & P_B \end{pmatrix} : \begin{pmatrix} |0,0\rangle \otimes |\pm\rangle \otimes |A\rangle \\ |1,\pm1\rangle \otimes |\mp\rangle \otimes |A\rangle \\ |1,0\rangle \otimes |\pm\rangle \otimes |A\rangle \\ |0,0\rangle \otimes |\pm\rangle \otimes |B\rangle \\ |1,\pm1\rangle \otimes |\mp\rangle \otimes |B\rangle \\ |1,0\rangle \otimes |\pm\rangle \otimes |B\rangle \end{pmatrix},$$

$$H_2^{\pm} = \begin{pmatrix} P_A + \frac{T_A}{2} & 4V_{pp\pi} + 4\alpha^2\Delta \\ 4V_{pp\pi} + 4\alpha^2\Delta & P_B + \frac{T_B}{2} \end{pmatrix} : \begin{pmatrix} |1,\pm1\rangle \otimes |\pm\rangle \otimes |A\rangle \\ |1,\pm1\rangle \otimes |\pm\rangle \otimes |B\rangle \end{pmatrix}. \tag{14}$$

Just as before, the blocks are doubly degenerate. The total Hamiltonian can be written as $H = H_1^+ \oplus H_1^- \oplus H_2^+ \oplus H_2^-$. From Eq. (13), one can see that at finite k, only $L_z = 0$ and $L_z \neq 0$ are coupled. This means that the degenerate eigenstates of H_2 blocks remain uncoupled since they are composed exclusively of $L_z \neq 0$ states.

The case of H_2 is slightly more complicated. The general form of the degenerate wave functions is

$$\begin{aligned} |\Psi^{\pm}\rangle = {} & a_A|0,0\rangle \otimes |\pm\rangle \otimes |A\rangle + b_A|1,\pm1\rangle \otimes |\mp\rangle \otimes |A\rangle \\ & + c_A|1,0\rangle \otimes |\pm\rangle \otimes |A\rangle + a_B|0,0\rangle \otimes |\pm\rangle \otimes |B\rangle \\ & + b_B|1,\pm1\rangle \otimes |\mp\rangle \otimes |B\rangle + c_B|1,0\rangle \otimes |\pm\rangle \otimes |B\rangle . \end{aligned} \tag{15}$$

Similarly to the M point, here we get

$$\begin{aligned} \langle\Psi^+|H|\Psi^-\rangle = {} & 4\sqrt{2}i\alpha k e^{-i\phi}\big[a_A b_B V_{sp\sigma}^{(1)} + a_B b_A V_{sp\sigma}^{(2)} \\ & + \beta\Delta(c_B b_A - c_A b_B)\big]. \end{aligned} \tag{16}$$

Despite being somewhat more elaborate compared to Eq. (10), Eq. (16) has the same form. The main difference between the two points of the Brillouin zone appears when the atoms of both sublattices are the same. In this case, $V_{sp\sigma}^{(1)} = V_{sp\sigma}^{(2)}$. Additionally, $a_A = -a_B$, $b_A = b_B$, and $c_A = c_B$, leading to a vanishing matrix element in Eq. (16). Thus, unlike the M point, where having a lattice composed of a single atomic type eliminates the spin texture while preserving the linear dispersion, Rashba-like dispersion at the Γ point requires two different atomic species.

IV. *AB INITIO* CALCULATIONS

We performed density functional theory (DFT) calculations implemented in QUANTUM ESPRESSO package [11] to simulate heavy elements BI, Pb, and Sn in a square lattice geometry. We employed projector augmeneted-wave (PAW) pseudopotential with Perdew-Burke-Ernzerhof (PBE) for the exchange and correlation functional within the generalized gradient approximation (GGA) [12]. The Kohn-Sham orbitals were expanded in a plane-wave basis with a cutoff energy of 70 Ry, and for the charge density a cutoff of 280 Ry was used. A k-point grid sampling grid was generated using the Monkhorst-Pack scheme with $16 \times 16 \times 1$ points [13]. For electronic band structure calculations, the spin-orbit interaction was included using noncollinear calculations with fully relativistic pseudopotentials. In Table I, we tabulate the optimized geometrical parameters of buckled heavy metal monolayers.

We use Rashba-like dispersion near the M point which is consistent with our TB prediction, shown in Fig. 2. In addition, since the A and B sublattices are composed of the same atomic species, there is no Rashba-like splitting at the Γ point.

In addition, we provide band structures of two lattices composed of two atomic species; see Fig. 2. As expected, breaking the species symmetry lifts the band degeneracy and introduces a Rashba-like dispersion at Γ.

V. DISCUSSION AND CONCLUSIONS

Having shown that buckled square lattices can give rise to Rashba-like bands, we now explain why the buckling of the system is a vital component. To keep the discussion as simple as possible, we focus on the M point.

Revisiting Eq. (9), we see that $|\Psi^{\pm}\rangle_{mn}$ contains the state $|1,0\rangle \otimes |m\rangle$ with the spin given by the superscript of Ψ. The fact that these two states are coupled to give rise to the linear dispersion means that there is a finite amplitude for spin-flipping processes for $|1,0\rangle$. The mechanism that allows the change of spin is spin-orbit interaction. To understand why buckling is required in addition to SOC, consider Fig. 3. This figure shows a set of steps describing a spin-flipping process. The path involves a transition between in-plane and out-of-plane orbitals of different atoms. From this illustration, it is clear why the lattice has to be buckled: In a flat lattice, p_z orbitals decouple from p_x and p_y, making the first hop impossible.

From our cartoon illustration in Fig. 3, it might appear that we have done unnecessary work by considering a square lattice because one only needs a zigzag 1D chain, similar to

TABLE I. Lattice constant a, buckling angle θ, buckling height d_z, and nearest-neighbor bond distance d.

	$2\alpha a$ (Å)	$\theta(^\circ)$	d_z (Å)	d (Å)
BiBi	3.89	30.3	3.04	3.19
PbPb	3.44	44.3	4.49	3.40
PbBi	3.63	38.4	3.84	3.26
PbSn	3.36	44.7	4.45	3.34

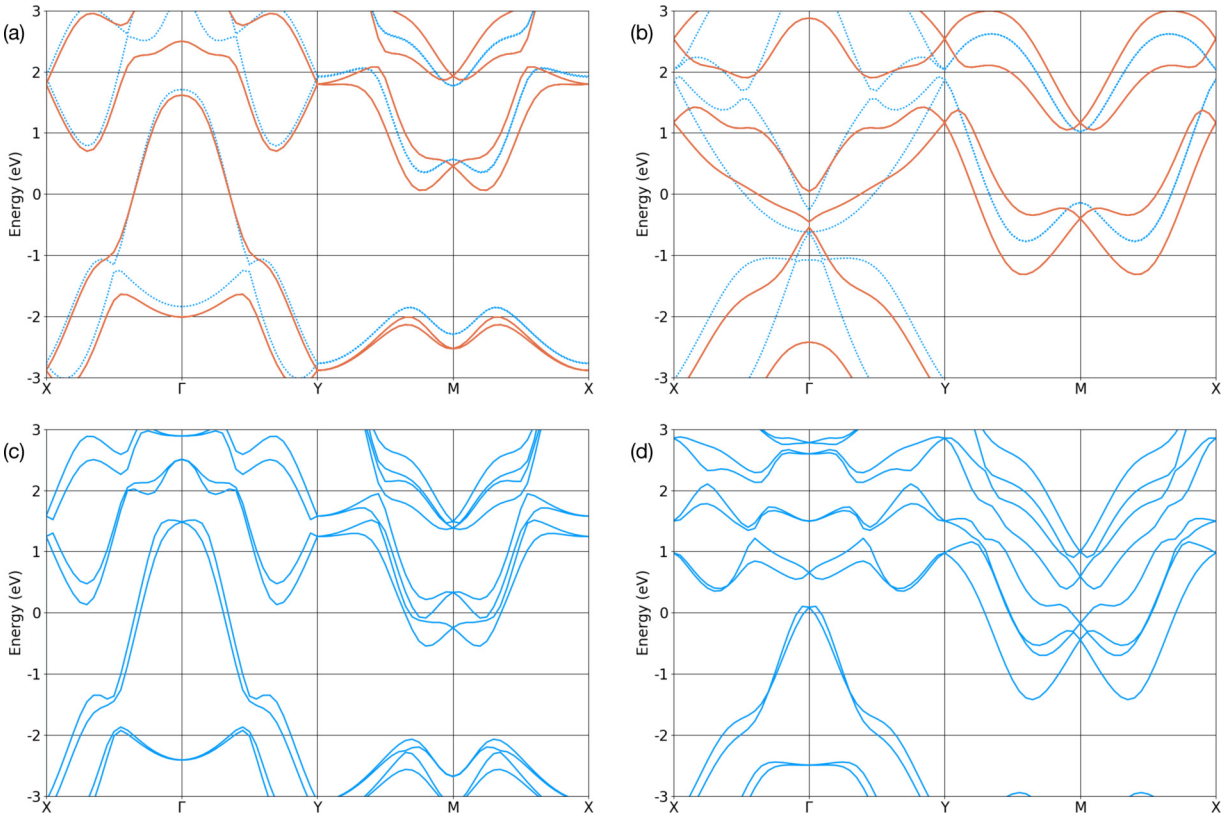

FIG. 2. Top row: band structures of Pb (a) and Bi (b). Fermi energy is set to be zero. Red lines indicate when spin-orbit interaction is included. Bottom row: Band structures for PbSn (c) and PbBi (d). Note the appearance of Rashba-like splitting at the Γ point and lifted degeneracy at the *M* point.

polyacetylene. It is possible to show that 1D chains are not sufficient by performing a full tight-binding analysis. However, an easier way to see that 1D chain is insufficient involves rotating it 90° around the longitudinal axis so that the zigzags are in the xy plane. In this orientation, p_z orbitals are decoupled and, as we determined above, one needs coupling between in-plane and out-of-plane orbitals to observe the SOI-induced band splitting.

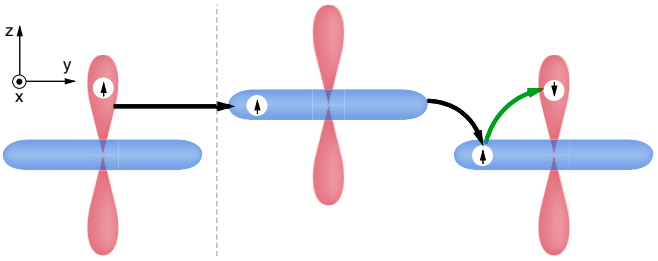

FIG. 3. Hopping path, leading to a spin-flip for an out-of-plane orbital. The first and third atoms belong to the same sublattice, and the middle one is a part of the other sublattice. The transition between the out-of-plane and in-plane orbitals is only allowed if the lattice is buckled. The transitions on the right-hand side of the dashed line take place within one eigenstate (e.g., $|\Psi^+\rangle_{mn}$). The hop across the dashed line is the transition between the two degenerate eigenstates of the Hamiltonian.

To summarize, we have shown that Rashba-like dispersion can arise in the absence of an external electric field in buckled materials with a strong spin-orbital coupling. The magnitude of the band splitting depends on the strength of the spin-orbit interaction and can reach the scale of electron volts for heavier atoms, making the spin texture separation stable against thermal fluctuations. This, along with the fact that the materials possess a fairly simple structure, makes them suitable candidates for spintronic applications.

ACKNOWLEDGMENTS

A.S.R., A.C., and A.H.C.N. acknowledge the National Research Foundation, Prime Minister's Office, Singapore, under its Medium-Sized Centre Programme and CRP award "Novel 2D materials with tailored properties: Beyond graphene" (No. R-144-000-295-281). The first-principles calculations were carried out at the Centre for Advanced 2D Materials and Graphene Research Centre high-performance computing facilities. P.Z.H., D.K.C., and H.S.P. acknowledge the support of the Physics and Mechanical Engineering Departments at Boston University and the Boston University High Performance Shared Computing Cluster. D.K.C. acknowledges the Aspen Center for Physics, which is supported by National Science Foundation Grant No. PHY-1607611, where part of this work was completed. P.Z.H is grateful for hospitality of the NUS Centre for Advanced 2D Materials and Graphene Research Centre, where this work was initiated.

[1] C.-C. Liu, H. Jiang, and Y. Yao, Phys. Rev. B **84**, 195430 (2011).
[2] C.-C. Liu, W. Feng, and Y. Yao, Phys. Rev. Lett. **107**, 076802 (2011).
[3] Y. Xu, B. Yan, H.-J. Zhang, J. Wang, G. Xu, P. Tang, W. Duan, and S.-C. Zhang, Phys. Rev. Lett. **111**, 136804 (2013).
[4] A. Kormányos, V. Zólyomi, N. D. Drummond, and G. Burkard, Phys. Rev. X **4**, 011034 (2014).
[5] A. Kormányos, G. Burkard, M. Gmitra, J. Fabian, V. Zlyomi, N. D. Drummond, and V. Falko, 2D Materials **2**, 022001 (2015).
[6] A. Molle, J. Goldberger, M. Houssa, Y. Xu, S.-C. Zhang, and D. Akinwande, Nat. Mater. **16**, 163 (2017).
[7] B. J. Wieder and C. L. Kane, Phys. Rev. B **94**, 155108 (2016).
[8] K. K. Gomes, W. Mar, W. Ko, F. Guinea, and H. C. Manoharan, Nature (London) **483**, 306 (2012).
[9] M. Polini, F. Guinea, M. Lewenstein, H. C. Manoharan, and V. Pellegrini, Nat. Nanotechnol. **8**, 625 (2013).
[10] J. C. Slater and G. F. Koster, Phys. Rev. **94**, 1498 (1954).
[11] P. Giannozzi, S. Baroni, N. Bonini, M. Calandra, R. Car, C. Cavazzoni, D. Ceresoli, G. L. Chiarotti, M. Cococcioni, I. Dabo *et al.*, J. Phys.: Condens. Matter **21**, 395502 (2009).
[12] J. P. Perdew, K. Burke, and M. Ernzerhof, Phys. Rev. Lett. **77**, 3865 (1996).
[13] H. J. Monkhorst and J. D. Pack, Phys. Rev. B **13**, 5188 (1976).